

# Identification of the High-affinity Substrate-binding Site of the Multidrug and Toxic Compound Extrusion (MATE) Family Transporter from *Pseudomonas stutzeri*<sup>\*[5]</sup>

Received for publication, March 22, 2016, and in revised form, May 27, 2016. Published, JBC Papers in Press, May 27, 2016, DOI 10.1074/jbc.M116.728618

Laiyin Nie<sup>†§1</sup>, Ernst Grell<sup>§</sup>, Viveka Nand Malviya<sup>§</sup>, Hao Xie<sup>§</sup>, Jingfang Wang<sup>‡2</sup>, and Hartmut Michel<sup>§3</sup>

From the <sup>†</sup>Tianjin University, School of Chemical Engineering and Technology, State Key Laboratory for Chemical Engineering, Collaborative Innovation Center of Chemical Science and Chemical Engineering, 300072 Tianjin, China and the <sup>§</sup>Department of Molecular Membrane Biology, Max Planck Institute of Biophysics, Max-von-Laue-Strasse 3, 60438 Frankfurt am Main, Germany

Multidrug and toxic compound extrusion (MATE) transporters exist in all three domains of life. They confer multidrug resistance by utilizing H<sup>+</sup> or Na<sup>+</sup> electrochemical gradients to extrude various drugs across the cell membranes. The substrate binding and the transport mechanism of MATE transporters is a fundamental process but so far not fully understood. Here we report a detailed substrate binding study of NorM\_PS, a representative MATE transporter from *Pseudomonas stutzeri*. Our results indicate that NorM\_PS is a proton-dependent multidrug efflux transporter. Detailed binding studies between NorM\_PS and 4',6-diamidino-2-phenylindole (DAPI) were performed by isothermal titration calorimetry (ITC), differential scanning calorimetry (DSC), and spectrofluorometry. Two exothermic binding events were observed from ITC data, and the high-affinity event was directly correlated with the extrusion of DAPI. The affinities are about 1  $\mu$ M and 0.1 mM for the high and low affinity binding, respectively. Based on our homology model of NorM\_PS, variants with mutations of amino acids that are potentially involved in substrate binding, were constructed. By carrying out the functional characterization of these variants, the critical amino acid residues (Glu-257 and Asp-373) for high-affinity DAPI binding were determined. Taken together, our results suggest a new substrate-binding site for MATE transporters.

The ability of all living organisms to protect themselves against toxic substances is essential for their survival. Organisms acquire this ability through evolutionary force (1). Due to the development of scientific knowledge, more and more medical drugs are being developed and applied. As a consequence, general defense mechanisms to resist antibiotics, drugs, and other toxic compounds have been evolved in bacteria (2). Being one of those defense mechanisms, the active extrusion of the toxic compounds from the cells plays an important role (3). In

bacteria, the extrusion is often carried out by multidrug transporters, which are integral membrane proteins. They are classified into five distinct families: ATP-binding cassette, multidrug and toxic compound extrusion (MATE),<sup>4</sup> major facilitator superfamily, resistance nodulation division, and small multidrug resistance transporters (4).

In 1999, the MATE family proteins were first recognized as a new group of the multidrug transporters, existing in all three domains of life (5). Most members of this family consist of a single chain of 450–550 amino acid residues and exhibit 12 putative transmembrane helices (TMHs). Up to now, about 900 proteins have been annotated as MATE transporters on the basis of amino acid sequence similarities. Moreover, a subclassification of the MATE family has been suggested, NorM-, DinF- (DNA damage-inducible protein F), and eukaryotic subfamily (4, 6, 7). Various compounds can be recognized by NorM proteins, including dyes, fluoroquinolones, and aminoglycosides (7). As secondary active transporters, MATE proteins utilize transmembrane Na<sup>+</sup> or H<sup>+</sup> electrochemical gradients to extrude toxic compounds.

So far atomic structures of four MATE transporters have been reported in their putative outward-facing states, in both drug-bound and/or drug-free states. NorM\_VC from *Vibrio cholerae* and NorM\_NG from *Neisseria gonorrhoeae*, are both Na<sup>+</sup> driven, whereas PfMATE from *Pyrococcus furiosus* and DinF-BH from *Bacillus halodurans* are published to be H<sup>+</sup>-dependent antiporters (8–11). All these four proteins contain 12 TMHs with intracellular N and C termini, and possess a hydrophobic internal cavity, formed by two symmetric bundles with 6 TMHs each. The two bundles are linked by a cytoplasmic loop between the 6th and 7th TMH. All MATE proteins share about 40% sequence similarity, and they employ the same rocker-switch mechanism for substrate extrusion (12). In addition, the crystal structures have also revealed different locations of cation- and substrate-binding sites, suggesting a mechanistic diversity among MATE transporters. In the structure of drug-bound NorM\_NG, the binding site is located close to the membrane-periplasm interface, whereas in the structure of PfMATE, the

<sup>\*</sup> This work was supported in part by the Max Planck Society, Deutsche Forschungsgemeinschaft Cluster of Excellence Frankfurt on Macromolecular Complexes Frankfurt and CRC 807, and International Science and Technology Cooperation Program of China Grant 2013DFE43150. The authors declare that they have no conflict of interest with the contents of this article.

<sup>[5]</sup> This article contains supplemental Table S1.

<sup>1</sup> Supported by the China Scholarship Council and the Max Planck Society.

<sup>2</sup> To whom correspondence may be addressed. Tel.: 86-2227405754; Fax: 86-2227374971; E-mail: wangjckh@tju.edu.cn.

<sup>3</sup> To whom correspondence may be addressed. Tel.: 49-6963031001; Fax: 49-6963031002; E-mail: hartmut.michel@biophys.mpg.de.

<sup>4</sup> The abbreviations used are: MATE, multidrug and toxic compound extrusion; TMH, transmembrane helix; TM, transmembrane;  $\beta$ -DDM, *n*-dodecyl  $\beta$ -D-maltoside; ITC, isothermal titration calorimetry; DSC, differential scanning calorimetry; CV, column volume(s); SEC-MALS, size-exclusion chromatography coupled to multi angle light scattering; Bistris, 2-[bis(2-hydroxyethyl)amino]-2-(hydroxymethyl)propane-1,3-diol; MIC, minimal inhibitory concentration.

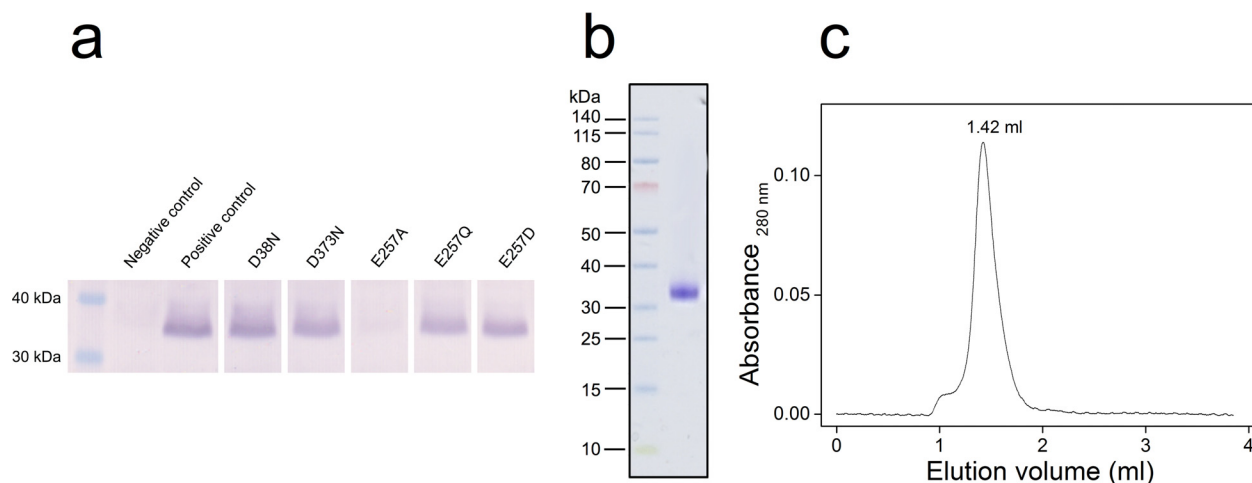


FIGURE 1. **Expression and purification of NorM\_PS and its variants.** *a*, Western blot of small scale expression screening of NorM\_PS and its variants in a *E. coli* KAM32 cell. The empty plasmid was used as negative control; induction of the WT as positive control. The samples were made out of 150  $\mu$ l of cell culture at  $A_{600} = 2$ . *b*, 10  $\mu$ g of purified NorM\_PS was loaded onto a 4–12% SDS-polyacrylamide gel, stained by Coomassie. *c*, analytical gel filtration profile of purified NorM\_PS using a Superdex 200 column in the NorM\_PS sample buffer.

drug binding pocket was published to be in the N-lobe cavity, which is halfway in the transmembrane region (9, 11). Despite the report of the crystal structures of MATE transporters, no detailed biochemical characterization and substrate binding studies have been performed so far. Only limited information is available regarding the binding affinity between MATE transporters and their substrates.

NorM\_PS, the subject of this study, is a MATE family transporter from *Pseudomonas stutzeri*, which can be considered to be an opportunistic but rare pathogen possessing a wide range of antibiotic resistance mechanisms (13). NorM\_PS contains 464 amino acid residues and is predicted to possess 12 TMHs. By conducting minimal inhibitory concentration (MIC) tests, we have shown that NorM\_PS functions as a multidrug transporter. The counter ion of substrate extrusion was identified to be  $H^+$ , determined by a transport assay employing everted membrane vesicles. Furthermore, detailed binding studies were performed between NorM\_PS and DAPI, a divalent cationic dye. Surprisingly, two binding events with different binding affinities were observed using isothermal titration calorimetry (ITC). The high-affinity binding event was substantiated by a fluorescence-based binding assay. Moreover, our results obtained by differential scanning calorimetry (DSC) measurements suggest a more compacted protein structure when DAPI is bound. Detailed studies on selected residues suggested that Asp-373 and Glu-257 are directly involved in high-affinity DAPI binding.

## Results

**Production and Purification of NorM\_PS and Its Variants—**Expression of NorM\_PS could be detected in the cell lysates by Western blot analysis with the anti-polyhistidine antibody. The protein band of NorM\_PS was found in the gel between 30 and 40 kDa (Fig. 1*a*). Of all the tested variants (D38N, E257A, E257Q, E257D, and D373N), E257A showed an undetectable expression level under our standard conditions (Fig. 1*a*), and all other variants could be produced in KAM32 cells with similar amounts as the wild-type (WT) protein.

NorM\_PS was purified using a combination of  $Ni^{2+}$ -affinity and size-exclusion chromatography in the presence of *n*-dode-

cyl  $\beta$ -D-maltoside ( $\beta$ -DDM). A single peak in the size exclusion chromatography indicated that NorM\_PS could be purified to homogeneity (Fig. 1*c*); the corresponding Coomassie-stained SDS-PAGE gel demonstrated a relatively high purity (Fig. 1*b*). A typical purification yielded up to 2.5 mg of NorM\_PS from 12 liters of cell culture. Among the tested variants, D38N, D373N, and E257D could be purified to a homogeneous state as the WT, whereas E257Q could not be isolated using our standard procedure, suggesting this residue is likely to play a critical role in maintaining the stability of NorM\_PS.

**The Oligomeric State of NorM\_PS—**Despite the difficulties in analyzing the oligomeric state of membrane proteins in detergent solution, it is essential to know this parameter for NorM\_PS to determine the quantitative thermodynamic parameters. In this study, we used size-exclusion chromatography coupled to multiangle laser light scattering (SEC-MALS) to study the oligomeric state of NorM\_PS, because this method has been successfully applied on many membrane proteins (14–19). Using a Superdex 200 column, the protein was eluted at 13.35 ml and showed a homogenous single peak detected by all three detectors (Fig. 2). The weight-averaged molecular mass was calculated based on the measured  $\Delta LS$  (light scattering) and  $C$  (the concentration of the protein) values (20). The molecular mass of NorM\_PS in detergent solution was determined to be 54.7 kDa, which corresponds well to the theoretical monomeric molar mass of 53.0 kDa. Surprisingly, the amount of detergent associated with NorM\_PS was quite high, the mass ratio between  $\beta$ -DDM and NorM\_PS ( $\delta$ ) was 2.82. This could be attributed to the high flexibility of NorM\_PS, so that more detergent is needed to stabilize the protein in solution.

**Drug Resistance of NorM\_PS—**NorM\_PS is annotated to be a multidrug transporter based on general sequence alignment. MIC tests were carried out to identify its potential substrates. The obtained MIC results are listed in Table 1. Elevated MIC values were observed for DAPI, doxorubicin, daunorubicin, tetracycline, kanamycin, and gentamycin, implying that *Escherichia coli* KAM32 cells harboring NorM\_PS exhibited a higher resistance to those toxic compounds. Among all tested compounds, the highest

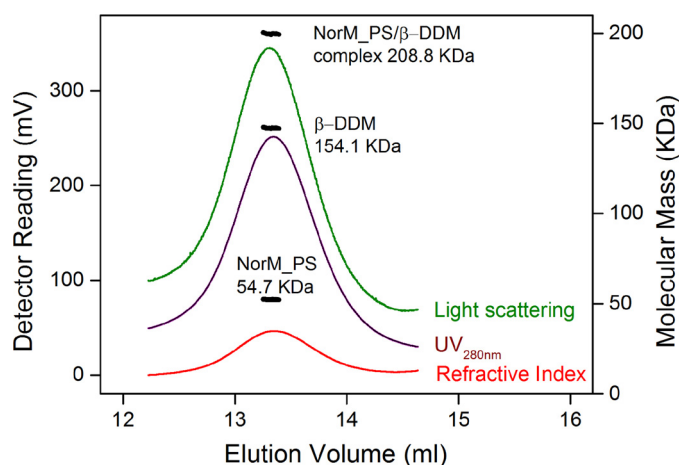


FIGURE 2. SEC-MALS analysis of NorM\_PS. The chromatogram shows the readings of the light scattering, refractive index, and UV detectors in green, red, and purple, respectively. The calculated molecular mass is shown on the right-hand axis. The thick black lines indicate the calculated molecular masses of the complete NorM\_PS-β-DDM complex, as well as the mass contributions of NorM\_PS and β-DDM components throughout the peaks. Three independent experiments were performed and the mean molecular mass of the protein was  $53.0 \pm 1.7$  kDa.

TABLE 1

MIC of various toxic compounds of NorM\_PS-expression KAM32 cells

Toxic Compounds	MIC	
	<i>E. coli</i> KAM32/pBADA2	<i>E. coli</i> KAM32/NorM_PS-pBADA2
DAPI	0.5	2
Doxorubicin	4	8
Daunorubicin	8	16
Tetracycline	0.25	0.5
Kanamycin	4	8
Gentamycin	2	4

relative resistance was observed for DAPI, so DAPI was chosen as a suitable and interesting substrate for further studies.

In this work, three residues (Asp-38, Glu-257, and Asp-383) were changed by mutagenesis, because they are acidic, located in the TM region (D38N in the N-bundle, E257D and D373N in the C-bundle), and are highly conserved within the NorM subfamily. As an initial screen, the MIC test was carried out for all 5 variants in the presence of DAPI. The extrusion of DAPI was totally abolished for these variants, because the MIC values were the same as the negative control, suggesting the critical role of these three residues.

**Cation Specificity of DAPI Antiport**—To obtain information on the driving force for the active extrusion, MIC tests were carried out using LB medium in the absence of NaCl and in the presence of DAPI. For control cells (KAM32 + empty pBADA2), the MIC value of DAPI in this selective medium was 0.25  $\mu\text{g/ml}$ , whereas the test cells (KAM32 + pBADA2-NorM\_PS) could tolerate up to 1.0  $\mu\text{g/ml}$  of DAPI. Using normal LB medium containing NaCl, both control and test cells could withstand DAPI concentrations up to 0.5 and 2.0  $\mu\text{g/ml}$  (Table 2). The reduced absolute MIC values in minimal medium could be the result of insufficient nutrients. However, the relative resistance between control and test cells in both media showed no dependence on the presence/absence of  $\text{Na}^+$ , excluding the possibility of considering  $\text{Na}^+$  as the counter ion of toxic compound extrusion.

TABLE 2

MIC values of DAPI determined in minimal media

Media	MIC	
	<i>E. coli</i> KAM32/pBADA2	<i>E. coli</i> KAM32/NorM_PS-pBADA2
LB	0.5	2
LB without NaCl	0.125	0.5

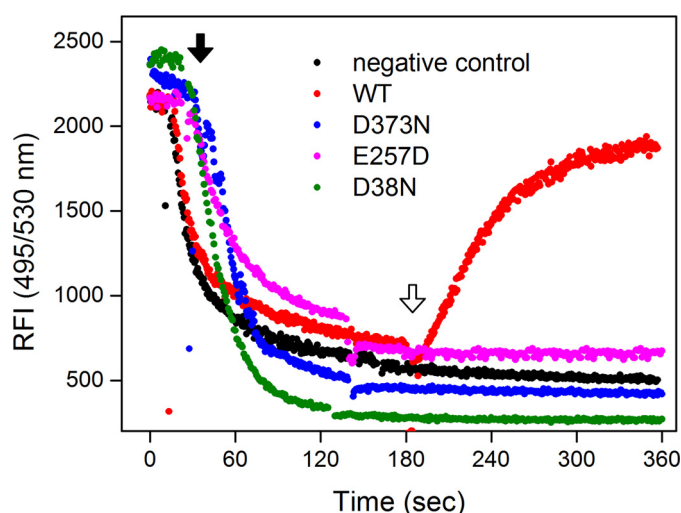


FIGURE 3. DAPI/ $\text{H}^+$  antiport assay using everted membrane vesicle. *E. coli* KAM32 cells with pBADA2 vector and pBADA2-NorM\_PS were employed to study the DAPI/ $\text{H}^+$  antiport. The fluorescence measurements were carried out with 400  $\mu\text{g}$  of total membrane proteins in a thermostated (25  $^{\circ}\text{C}$ ), stirred cuvette containing 2  $\mu\text{M}$  acridine orange in 1 ml of modified TCS buffer (5 mM Tris-HCl, 140 mM choline chloride, 5 mM  $\text{MgCl}_2$ ). Vesicles were preloaded with protons by addition of 10 mM Na-DL-lactate (solid arrow), and the proton transport was initiated by 50  $\mu\text{M}$  DAPI (open arrow). The excitation and emission wavelengths are 495 and 530 nm, respectively.

To confirm the ion specificity for  $\text{H}^+$ , a DAPI/ $\text{H}^+$  antiport assay employing everted membrane vesicles was implemented. Acridine orange was chosen as a probe to monitor  $\text{H}^+$ . Because this fluorescent dye is membrane permeable in its deprotonated form and, if a pH gradient is established, will accumulate in their protonated form and get quenched on the side of the membranes where the pH is lower (21). In a typical measurement, upon addition of lactate (solid arrow in Fig. 3), the respiration was initiated and thus a pH gradient (acidic inside) was generated as monitored by the quenching of the fluorescence. The addition of DAPI (open arrow in Fig. 3) caused an increase in fluorescence intensity (red dots in Fig. 3), suggesting an efflux of  $\text{H}^+$  from the cytoplasm to periplasm in overproduced NorM\_PS-containing membrane vesicles elicited by DAPI, which clearly suggested the DAPI/ $\text{H}^+$  antiport. By contrast, everted membrane vesicles in the absence of NorM\_PS showed no response to DAPI (black dots in Fig. 3). Taken together, our data support that NorM\_PS functions as an  $\text{H}^+$ -dependent transporter.

In addition to the WT protein, the transport assay was performed with D38N, D373N, and E257D. No fluorescence intensity increase upon DAPI addition was observed, suggesting that  $\text{H}^+$  could not be translocated (Fig. 3).

**Differential Scanning Calorimetry**—To obtain information about thermal stability, general structural features related to DAPI binding behavior of NorM\_PS, a DSC study was per-



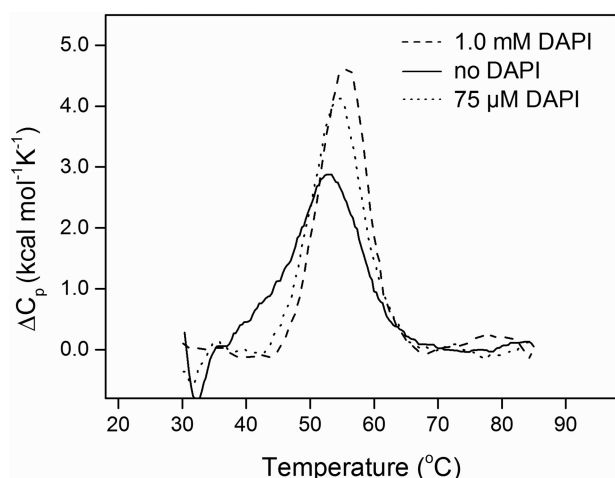


FIGURE 4. DSC profile of NorM\_PS (25  $\mu\text{M}$ ) in the absence (solid line) and presence of 75  $\mu\text{M}$  (dot line) as well as 1.0 mM (dash line) DAPI in 20 mM HEPES-NaOH, pH 7.5, adjusted with sodium lactate to total ionic strength of 20 mM. Transition temperatures, enthalpy changes, and widths at half-maximum height are: 53.5  $^{\circ}\text{C}$ , 40.0  $\text{kcal mol}^{-1}$ , 13.5  $^{\circ}\text{C}$ ; 54.5  $^{\circ}\text{C}$ , 41.5  $\text{kcal mol}^{-1}$ , 10.0  $^{\circ}\text{C}$ ; and 56.0  $^{\circ}\text{C}$ , 42.0  $\text{kcal mol}^{-1}$ , 8.5  $^{\circ}\text{C}$ , respectively.

TABLE 3

DSC data (mean values) of NorM\_PS in presence and absence of DAPI

10 to 30  $\mu\text{M}$  NorM\_PS was measured in 20 mM HEPES-NaOH, pH 7.4, adjusted to ionic strength, 20  $\pm$  3 mM with sodium lactate.

$C_{\text{DAPI}}$	$T_m$	$\Delta H$	WHMH <sup>a</sup>	$n^b$
mm	$^{\circ}\text{C}$	$\text{kcal mol}^{-1}$	$^{\circ}\text{C}$	
0	52.5 $\pm$ 2.0	39.5 $\pm$ 4	12.5 $\pm$ 1.0	6
0.075	55.0 $\pm$ 0.5	43.0 $\pm$ 4.5	9.5 $\pm$ 0.8	3
1.1 $\pm$ 0.1	55.0 $\pm$ 0.5	45.0 $\pm$ 4.5	8.5 $\pm$ 0.5	5

<sup>a</sup> WHMH, width of transition at half-maximum height.

<sup>b</sup>  $n$ , number of experiments performed.

formed at pH 7.4 and at constant ionic strength in the temperature range between 10 and 85  $^{\circ}\text{C}$ . The protein samples exhibited an irreversible endothermic transition at around 53  $^{\circ}\text{C}$ . In the absence of ligand (solid line in Fig. 4), a very broad, almost symmetric transition of NorM\_PS with a maximum at 53.5  $^{\circ}\text{C}$  was recorded. In the presence of 1 mM DAPI, the transition temperature was increased about 3  $^{\circ}\text{C}$  on average (Table 3). A very characteristic change, however, was the marked decrease of the width of the protein transition in the presence of DAPI (Fig. 4, Table 3), observed for all protein samples. The small change in thermal stability as indicated by the increase of transition temperature and the marked decrease of the transition width provides strong evidence for DAPI binding to NorM\_PS.

**Spectrofluorometric Titration**—DAPI is twice positively charged at physiological pH and has been widely applied for DNA detection in biology due to its fluorescent properties (22). Besides, the interaction between DAPI and negatively charged proteins and lipid vesicles has been investigated (23, 24). In general, DAPI binding was associated with a blue shift of the emission spectrum and a marked increase of the emission intensity. There are two different rotamers of DAPI in solution and only one undergoes an intramolecular proton transfer, from the 6-amidinium group to the indole aromatic ring, in the excited singlet state of DAPI alone (23). However, upon binding to BSA and DNA or when dissolved in DMSO, this transfer does not occur and consequently causes a large increase of fluorescence (23).

In this study, we observed that the fluorescence intensity of DAPI increased upon the addition of NorM\_PS (Fig. 5a), which we attribute to binding. Meanwhile, the excitation maximum of DAPI at 345 nm exhibited a 14-nm red shift in the presence of NorM\_PS, whereas the main emission maximum at 465 nm was blue shifted

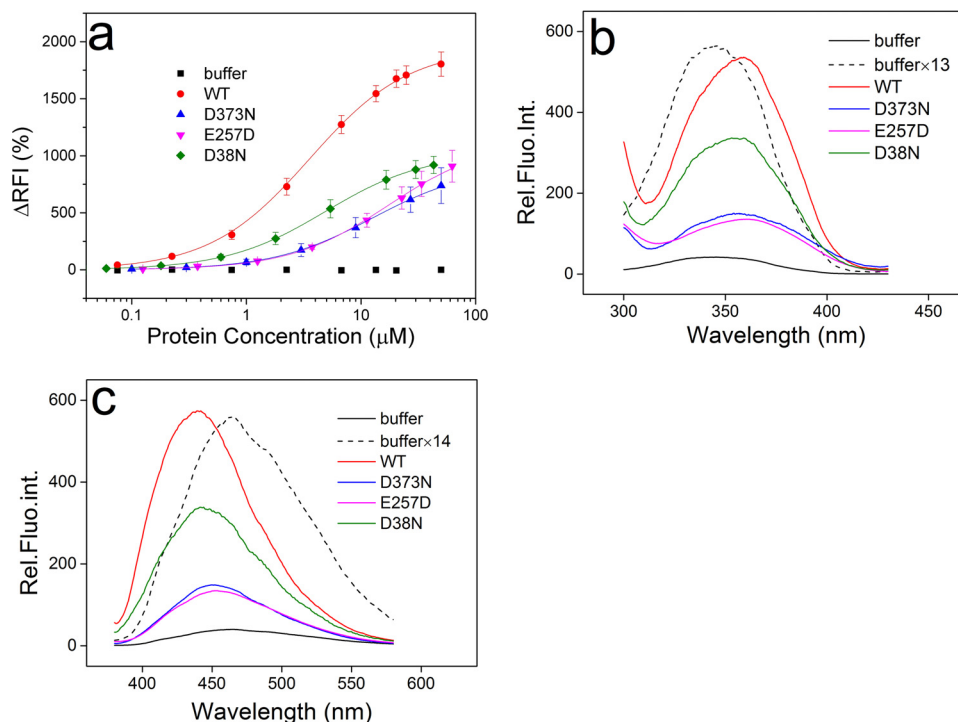


FIGURE 5. Spectrofluorometric titration of 0.5  $\mu\text{M}$  DAPI in the presence of NorM\_PS and its variants. *a*, the concentrated protein sample (up to 250  $\mu\text{M}$ ) was titrated into 20 mM HEPES-NaOH, 0.025% (w/v)  $\beta$ -DDM, 0.5  $\mu\text{M}$  DAPI, 11 mM sodium lactate, pH 7.4. The titration experiments were repeated three times. *b*, excitation ( $E_m$  = 450 nm) and *c*, emission ( $E_x$  = 360 nm) spectra of DAPI in the absence (black) and presence of 50  $\mu\text{M}$  different proteins.

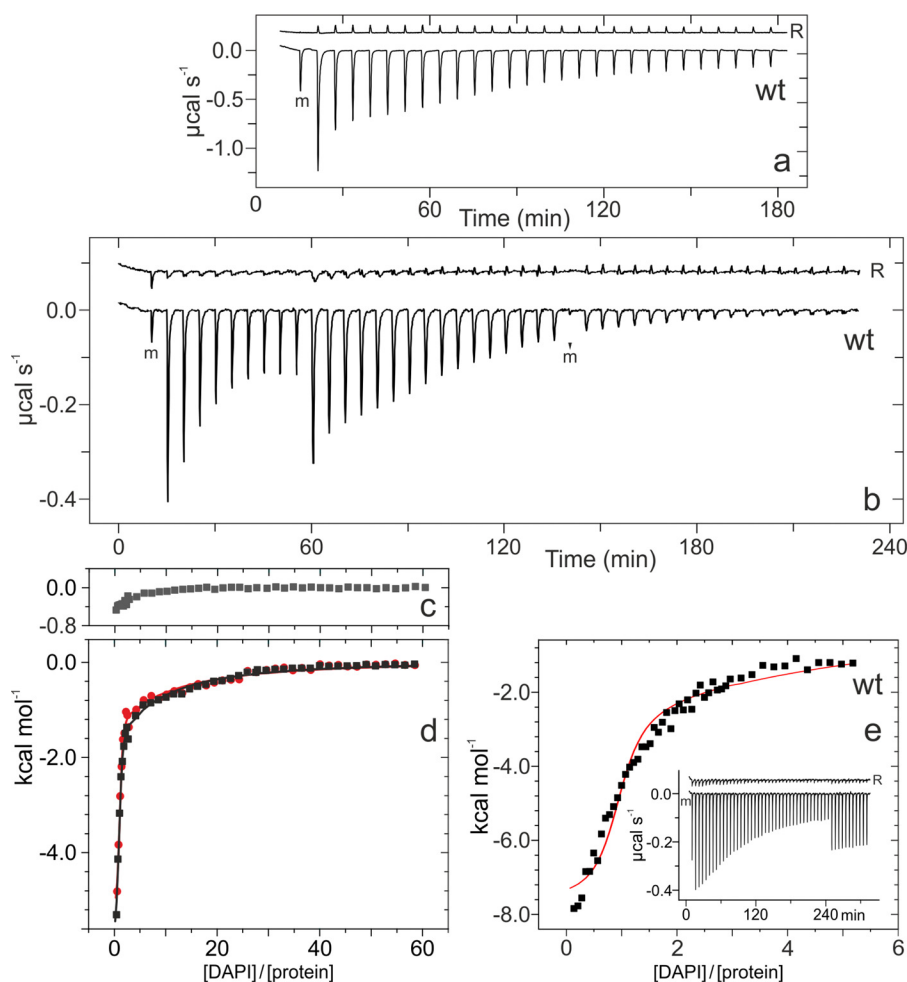


FIGURE 6. DAPI binding to NorM\_PS studied by ITC at 25 °C in 20 mM HEPES-NaOH, 0.025% (w/v)  $\beta$ -DDM, pH 7.4,  $I = 20$  mM (sodium lactate). *a*, titration of 6  $\mu$ M protein with 1.5 mM DAPI and reference titration *R* (offset shifted). Injections were 4  $\mu$ l (m) + 26  $\times$  10  $\mu$ l. *b*, combined titration of 4  $\mu$ M protein with 0.5 mM DAPI and corresponding reference titration *R* (offset shifted). Injections were 3  $\mu$ l (m) + 12  $\times$  6  $\mu$ l + 11  $\times$  18  $\mu$ l, 3  $\mu$ l (m) + 15  $\times$  18  $\mu$ l. *c*, integrated reference titration (from *b*), heat change plotted versus concentration ratio. *d*, integrated protein titration (from *b*) after reference subtraction according to modes i (red dots) and ii (black squares), solid curves are the corresponding evaluation (parameter list in Table 5, and mean values from 3 measurements are in Table 4). *e*, integrated 12  $\mu$ M protein with 0.3 mM DAPI titration (parameters are listed in Table 4), the protein and corresponding reference titration are shown as an inset. Injections were 4  $\mu$ l (m) + 39  $\times$  4  $\mu$ l + 11  $\times$  10  $\mu$ l.

by 25 nm (Fig. 5, *b* and *c*). The fluorescence changing and shifting also clearly indicate binding of DAPI to NorM\_PS.

To determine the binding affinity, spectrofluorometric titrations were carried out (Fig. 5*a*). This determination was done under conditions where the total absorbance at the excitation wavelength (360 nm) did not exceed 0.09 per 0.5-cm light path, which allowed neglecting of the 1st order filter effect. At concentrations of NorM\_PS above 10  $\mu$ M, the titration exhibited a tendency of saturation. An evaluation of four titrations based on a 1:1 stoichiometry provided a mean dissociation constant ( $K_d$ ) of  $3.5 \pm 1.0$   $\mu$ M (Fig. 5*a*), which corresponded well to the high-affinity binding observed by the ITC measurements (see the ITC results below for details).

The DAPI binding study was carried out with variants D38N, E257D, and D373N. Being negatively charged in their deprotonated form and located halfway in the TMHs, these residues could also be involved in DAPI binding. Within the same concentration range, E257D and D373N behaved differently from the WT protein. The blue shift in the emission spectra decreased from 25 to 13 nm. Apart of this smaller spectral shift, the emission was

smaller than for the WT protein (Fig. 5*c*). The determination of a  $K_d$  value was not possible due to the absence of an apparent saturation (up to 60  $\mu$ M). This observation likely indicates that both variants, E257D and D373N, are still somehow able to bind to DAPI but not with high affinity.

In contrast to E257D and D373N, the excitation and emission maxima of DAPI in the presence of D38N were similar to those of the WT protein and the titration also exhibited saturation behavior. The calculated  $K_d$  value of D38N was  $4.9 \pm 1.0$   $\mu$ M (3 titrations). On the other hand, the emissions of titrations with D38N were significantly lower than in the case of the WT protein (Fig. 5*a*). This observation could be due to a change within the local surrounding of the fluorophore when bound to D38N.

**Isothermal Titration Calorimetry**—To achieve more insights into DAPI binding to NorM\_PS and the related energetic aspects, a detailed ITC study was carried out at 25 °C at constant ionic strength in the NorM\_PS sample buffer,  $I = 20$  mM (sodium lactate), unless specified differently. The general titration behavior is shown in Fig. 6*a*. Here, the dominating and resolved exothermic titration process was characterized by a  $K_d$

TABLE 4

Thermodynamic parameters (mean values) for DAPI binding to NorM\_PS and its variants

Data were measured at 25 °C in 20 mM HEPES-NaOH, 0.025% (w/v) DDM, pH 7.4, adjusted to ionic strength 20 or 100 mM with sodium lactate; for clarity, the association constant and entropy change for the measurements are shown in Table 5.

Protein	N1 <sup>a</sup>	<i>K<sub>a</sub></i> 1 <sup>b</sup>	<i>K<sub>d</sub></i> 1 <sup>b</sup>	$\Delta H1$	$\Delta S1$	N2 <sup>a</sup>	<i>K<sub>a</sub></i> 2 <sup>b</sup>	<i>K<sub>d</sub></i> 2 <sup>b</sup>	$\Delta H2$	$\Delta S2$
		$\mu\text{M}^{-1}$	$\mu\text{M}$	$\text{kcal mol}^{-1}$	$\text{cal mol}^{-1} \text{K}^{-1}$		$\text{mM}^{-1}$	$\text{mM}$	$\text{kcal mol}^{-1}$	$\text{cal mol}^{-1} \text{K}^{-1}$
WT	1	1.5 ± 0.6	0.67	-6.3 ± 3.0	7	2	5.5 ± 1.5	0.18	-45 ± 35	-134
	0.91 ± 0.03	1.1 ± 0.2	0.91	-9.0	-3	2	2.4 ± 1.5	0.42	-77 ± 20	-245
	1 <sup>c</sup>	0.22 ± 0.15	4.5	-3.6 ± 1.0	12	2	0.9 ± 0.5	1.1	-32 ± 20	-94
D38N	1	0.27 ± 0.15	3.7	-3.9 ± 1.5	12	2	12 ± 3	0.083	-35 ± 20	-99
D373N	1	0.052 ± 0.025	19	3.0 ± 1.5	4	2	3.9 ± 1	0.26	-43 ± 5	-128
E257D	1	0.085 ± 0.05	12	5.4 ± 2.0	41	2	4.8 ± 2	0.21	-78 ± 20	-245

<sup>a</sup> N, stoichiometric coefficient; assumed values in bold italics.<sup>b</sup> *K<sub>a</sub>*, association constant; *K<sub>d</sub>*, dissociation constant; *K<sub>d</sub>* = *K<sub>a</sub>*<sup>-1</sup>.<sup>c</sup> Titration was performed at 100 mM ionic strength; all the other titrations were performed at 20 mM ionic strength.

of about 0.1 mM. However, the 1st full DAPI injection, following “m,” exhibited a surprisingly large heat change (Fig. 6*a*), which may be assigned to an unresolved, additional exothermic binding process of higher affinity.

Another unexpected observation was made during the starting phase of reference titrations “R” (Fig. 6*b*, full additions 1 to 14). Reference titrations are usually expected to show only comparatively narrow signals of similar magnitude due to the quickly equilibrating heat changes. The observed exothermic, broad signal could be attributed to a chemical process such as a de-aggregation of DAPI upon dilution. This process was independent of the presence of detergent in the buffer, its ionic strength, and the stirring rate (data not shown). If this process is assigned, for example, to a dissociation of DAPI dimers, the related dimer/monomer dissociation constant is around 25  $\mu\text{M}$  and the enthalpy change around -2  $\text{kcal mol}^{-1}$ , a result of a separate investigation. Ligand dilution together with the de-aggregation process contributed also to the titrations in the presence of NorM\_PS (Fig. 6, *b* and *c*), which are assumed to be additive for the purpose of evaluation. For this study, the aggregated form of DAPI is considered as reference state for the evaluations. Nevertheless, we assume that only DAPI monomers are bound to NorM\_PS and its variants. The thermodynamic parameters resulting from our evaluations are apparent ones, characteristic for our experimental conditions.

For the WT protein titration, an exothermic binding of DAPI to NorM\_PS with an affinity higher than 0.1 mM (Fig. 6*a*) was resolved by carrying out titrations with lower DAPI concentration and by adding different ligand volumes (Fig. 6*b*). The titration in Fig. 6*b* represents a combination of two successive titrations using the same titrant concentration, combined using the program CONCAT. To subtract the reference titration data, two different modes were applied: (i) by subtracting the non-uniform reference titration in the integrated form (Fig. 6*c*) and (ii) by subtracting a nearly constant value characterizing merely the mean heat of dilution. The resulting heat changes ( $\Delta q$ ) in dependence of the DAPI/protein concentration ratio, obtained by employing both subtraction modes i and ii, were applied for final evaluations (Fig. 6*d*). Both resulting point sequences clearly revealed two distinct binding phases, a very steep phase characterizing high-affinity and a gradually growing one characteristic of low-affinity binding.

The evaluation method to obtain thermodynamic parameters was based on the “two binding sites” model, in which two types of independent sites for high- and low-affinity binding

were taken into consideration. Even if N1 (stoichiometric coefficient for high-affinity binding) and N2 (stoichiometric coefficient for low-affinity binding) were set equal 1, still at least four parameters (the dissociation constants *K<sub>d</sub>*1 and *K<sub>d</sub>*2, and the enthalpy changes  $\Delta H1$  and  $\Delta H2$ ), had to be determined. No direct fits could be achieved under such circumstance using the standard evaluation program. Therefore, a partial analysis of the high- and low-affinity parts of the titration in Fig. 6*d* was carried out separately, with N1 and N2 fixed to 1. Subsequently, the obtained parameters were used to do simulations related now to the complete titration. The resulting parameters finally could be used as suitable starting values to achieve possible solutions.

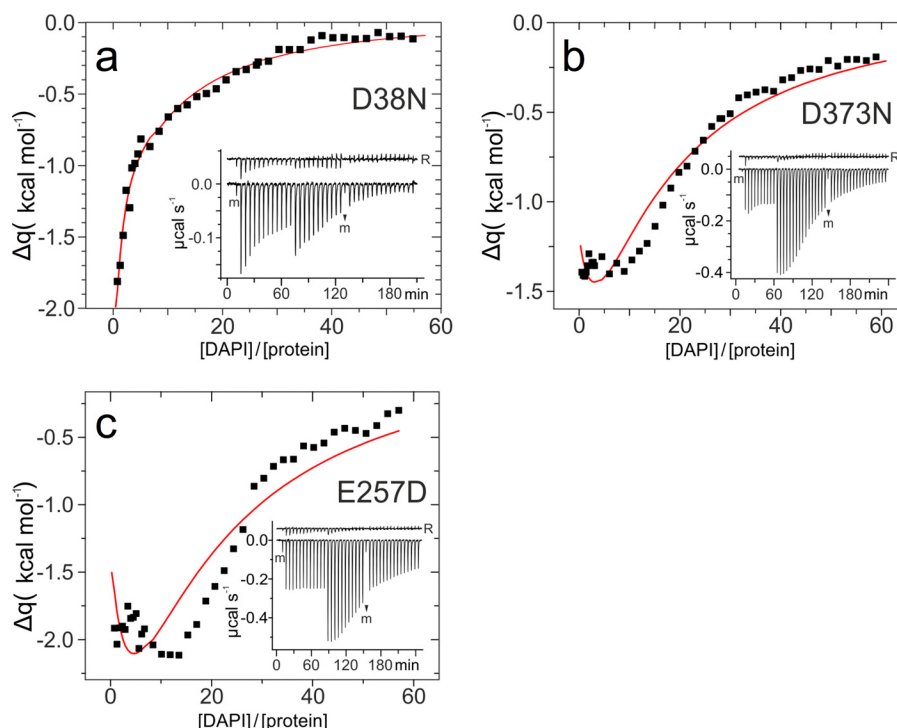
For the titration in Fig. 6*d*, high-affinity binding (1:1 complex) is characterized by a *K<sub>d</sub>*1 value around 0.95  $\mu\text{M}$  and a  $\Delta H1$  value of about -7.2  $\text{kcal mol}^{-1}$ , and a very low value for  $\Delta S1$ . Cratic entropy is not considered in this study. For low-affinity binding (N2 = 1), *K<sub>d</sub>*2 and  $\Delta H2$  values of around 0.13 mM and -78  $\text{kcal mol}^{-1}$ , respectively, were obtained. This  $\Delta H2$  value is extremely high for the binding of a single ligand. We assume therefore, for low-affinity binding, that at least two DAPI molecules were bound per NorM\_PS (N2 = 2), leading to a  $\Delta H2$  value of -39  $\text{kcal mol}^{-1}$ . The complete set of parameters including errors obtained for the titration shown in Fig. 6*d* is given in Table 5. All subsequent low-affinity data for the WT protein and its variants were given for N2 = 2. The mean values of the thermodynamic parameters, based on subtraction mode i, resulting from several independent experiments are listed in Table 4. The reference subtraction mode i was considered to be more realistic due to the chemical process of DAPI de-aggregation, so it was used for all the data analysis. Nevertheless, adopting mode ii, similar results were obtained (Table 5).

It is important to determine experimentally the value of the stoichiometric coefficient N1 for high-affinity DAPI binding. Therefore, a detailed high-affinity titration with 12  $\mu\text{M}$  NorM\_PS up to a DAPI/protein concentration ratio of about 5.5 was carried out (Fig. 6*e*). The evaluation could only be successfully performed when  $\Delta H1$  was fixed, and a value of 0.91 was resulted for N1. The number of -9  $\text{kcal/mol}$  for  $\Delta H1$  was used based on a simulation performed on this dataset. This supports our earlier assumption that for high-affinity binding a 1:1 DAPI-protein complex is formed under saturating conditions. The initially assumed N1 value of 1 will from now on be used for all subsequent calculations.

If the high-affinity DAPI binding is dominated by electrostatic interactions, an increase of the ionic strength should lead

**TABLE 5****Thermodynamic parameters for DAPI binding to NorM\_PS and its variants**All the fits were performed with fixed  $N1 = 1$ ,  $N2 = 2$ .

Protein (Figure)	$K_a1$	$\Delta H1$	$\Delta S1$	$K_a2$	$\Delta H2$	$\Delta S2$
	$\mu\text{M}^{-1}$	$\text{kcal mol}^{-1}$	$\text{cal mol}^{-1} \text{K}^{-1}$	$\text{mM}^{-1}$	$\text{kcal mol}^{-1}$	$\text{cal mol}^{-1} \text{K}^{-1}$
WT (Fig. 6d)	$1.1 \pm 0.6^a$	$-7.2 \pm 0.8$	3.5	$7.9 \pm 1.4$	$-39 \pm 4.1$	-114
	$0.99 \pm 0.51^b$	$-7.8 \pm 0.8$	1.4	$9.3 \pm 1.3$	$-40 \pm 3.2$	-117
D38N (Fig. 7a)	$0.4 \pm 0.2$	$-3.0 \pm 0.7$	16	$9.5 \pm 1.5$	$-16 \pm 1.1$	-38.0
D373N (Fig. 7b)	$0.05 \pm 0.008$	2	28	$4.4 \pm 2.2$	$-41 \pm 2.2$	-122
E257D (Fig. 7c)	$0.06 \pm 0.007$	6	44	$4.6 \pm 1.0$	$-90 \pm 10$	-280

<sup>a</sup> Data were evaluated using reference subtraction mode i, all the other experiments in this table were evaluated using this mode.<sup>b</sup> Data were evaluated using reference subtraction mode ii.

**FIGURE 7. DAPI binding to variant D38N and D373N by ITC at 25 °C in the medium of Fig. 6.** *a*, combined titration of 4  $\mu\text{M}$  D38N with 0.5 mM DAPI and corresponding reference titration *R* (offset shifted) as shown in the *inset*; heat change after subtraction of reference titration plotted versus concentration ratio (parameter list in Table 5 and mean values of 3 measurements are listed in Table 4). Injection was 3  $\mu\text{l}$  (m) + 12  $\times$  6  $\mu\text{l}$  + 11  $\times$  18  $\mu\text{l}$ , 3  $\mu\text{l}$  (m) + 15  $\times$  18  $\mu\text{l}$ . *b*, combined titration of 6.0  $\mu\text{M}$  D373N with 0.8 mM DAPI and corresponding reference titration *R* (offset shifted) as shown in the *inset*; heat change after subtraction of reference titration plotted versus concentration ratio and evaluated on the basis of model NSe (parameter list in Table 5 and mean values of 2 measurements are listed in Table 4). Injection was 3  $\mu\text{l}$  (m) + 9  $\times$  3  $\mu\text{l}$  + 16  $\times$  15  $\mu\text{l}$ , 3  $\mu\text{l}$  (m) + 17  $\times$  15  $\mu\text{l}$ . *c*, combined titration of 4  $\mu\text{M}$  E257D with 0.5 mM DAPI and corresponding reference titration *R* (offset shifted) as shown in the *inset*; heat change after subtraction of reference titration plotted versus concentration ratio (parameter list in Table 5 and mean values of 2 measurements are listed in Table 4). Injections were 3  $\mu\text{l}$  (m) + 12  $\times$  6  $\mu\text{l}$  + 11  $\times$  18  $\mu\text{l}$  and 3  $\mu\text{l}$  (m) + 15  $\times$  18  $\mu\text{l}$ .

to an increased shielding of the involved charges. Therefore, high-affinity binding would be expected to be weaker at high ionic strength ( $>20$  mM). This expectation was indeed confirmed qualitatively by the result of our titration at  $I = 100$  mM (sodium lactate), given in Table 4 (titration not shown).

The calorimetric titration was performed with the three variants, D38N, D373N, and E257D. The titration pattern of D38N is very similar to that of the WT protein, the two characteristic phases of exothermic high- and low-affinity binding were clearly observed (Fig. 7a). The resulting thermodynamic parameters (Table 4) are close to those of the WT protein, only that the  $K_a1$  value is slightly higher. The masking of the negative side chain charge of Asp-38 did not markedly influence the binding behavior, indicating that Asp-38 is not directly involved in high-affinity DAPI binding.

Unlike D38N, in the case of the variant D373N, the characteristic initial, strong exothermic high-affinity binding almost

disappeared, whereas the low-affinity binding still remained (Fig. 7b). For data evaluation, proper fit could be achieved by using either fixed  $K_a1$  or  $\Delta H1$  value (solid line in Fig. 7b). The  $K_a1$  value is higher than that in the case of the WT and D38N, and the binding became entropy driven due to the positive  $\Delta H1$  and  $\Delta S1$  values; for low-affinity DAPI binding, the mean parameters essentially correspond to those mentioned before (Table 4). However, the contribution of the low-affinity binding below the DAPI/protein concentration ratio around 12 was missing because the first 10 equal DAPI additions led to heat changes of similar magnitude (*inset* in Fig. 7b). This unexpected point sequence can be attributed to a superposition of an endothermic binding process and the initial part of the exothermic low-affinity binding process. As a consequence, Asp-373 can be assumed to be involved in DAPI binding.

For E257D, the combination of two titrations showed a behavior close to that of D373N (Fig. 7c), and the calculated



thermodynamic parameters were also similar (Table 4), only that the enthalpy and entropy changes for the low-affinity binding were larger than those for D373N. This observation may be due to the fact that a single binding equilibrium related to only one dissociation constant may not be suitable to describe low-affinity ligand binding to E257D quantitatively. However, similar titration behavior as D373N regarding the high-affinity binding might indicate a direct participation of Glu-257 in high-affinity DAPI binding.

### Discussion

#### Physicochemical and Biochemical Aspects

**NorM\_PS Is a Multidrug/H<sup>+</sup> Antiporter**—In this study, we characterized a multidrug transporter from *P. stutzeri*. The drug-hypersusceptible *E. coli* strain KAM32 overexpressing NorM\_PS displays increased resistance to 6 toxic compounds, which demonstrates that the protein functions as a toxin extruder *in vivo*. NorM\_PS exhibits a moderate level of cellular resistance against substrates (2–4-fold), which is in accordance with former studies on MATE transporters (10, 25). The low level of cellular resistance might be due to low expression levels of transporters (10), however, so far this suggestion could not be substantiated by experimental results. Moreover, based on sequence similarities, the MATE family belongs to the multidrug/oligosaccharidyl-lipid/polysaccharide (MOP) exporter superfamily (TCDB 2.A.66), sharing a certain similarity as the prokaryotic polysaccharide transporter family. The prokaryotic polysaccharide transporter family is known to be involved in the lipopolysaccharide O-antigen repeat unit as well as exopolysaccharide or capsular polysaccharide export in bacteria (26). Instead of extruding drugs or toxic compounds like DAPI, the MATE transporters from bacteria might play an important role in the extrusion of lipid precursors or metabolic waste products. It therefore might be comprehensible that MATE transporters from bacteria confer only modest multidrug resistance.

With regard to ion specificity of NorM\_PS, our results support that NorM\_PS utilizes the H<sup>+</sup> potential across the membrane as its energy source, and no signs of simultaneous Na<sup>+</sup> coupling have been observed. The result of the MIC tests in Na<sup>+</sup>-deficient medium showed no difference to that in normal LB, proving that Na<sup>+</sup> did not affect the function of NorM\_PS *in vivo*. In the *in vitro* ITC experiment, Na<sup>+</sup> was titrated into purified NorM\_PS up to a molar ratio of 1600, but no sign of binding could be observed (data not shown). Among all functionally characterized NorM subfamily proteins, most confer a Na<sup>+</sup> dependence, only NorM\_PS from *P. stutzeri*, PmpM (homologue of NorM\_PS) from *Pseudomonas aeruginosa*, and AbeM from *Acinetobacter baumannii* show an ion specificity for H<sup>+</sup>. Particularly, NorM\_VC, previously assumed to be Na<sup>+</sup> dependent, was reported of being able to simultaneously bind Na<sup>+</sup> and H<sup>+</sup> (27). This diversity of the counter cation for substrate extrusion shows a high adaptability of MATE transporters.

**Qualitative Ligand Binding**—After incubating with DAPI, the peak width at half-maximum intensity of the thermal NorM\_PS transition decreases dramatically in DSC, which is usually a sign of a more compacted structure. Thus, there is likely to be a conformational change induced by DAPI binding.

As for the local surroundings of bound DAPI, some insights could be obtained by comparing its fluorescence spectra with those of the fluorophore in different media.

For this purpose, the influence of solvent polarity on the fluorescence properties of free DAPI, its excitation and emission spectra were measured in water, methanol, and isopropyl alcohol. Decreasing polarity of the solvent leads to an increase of the red shift of the excitation and a blue shift of the emission maximum together with an increase of emission intensity (data not shown). The same changes were observed when DAPI was bound to the WT protein and the variant D38N (Fig. 5, *a–c*). This observation is considered as an indication that the aromatic residues of bound DAPI are preferentially located in a rather nonpolar environment of the protein such as between amino acid side chains of the hydrophobic TM region.

Another unexpected observation in our substrate binding study is the additional low-affinity binding. In general we consider the low-affinity binding event to be qualitatively characterized, the calculated binding affinity has more significance in terms of the range rather than the exact number itself. Although the transfer of DAPI across the TM region of the protein may require more than one binding site, it appears unlikely to us, to assign more than one postulated site to the TM region of NorM\_PS. The observed large  $\Delta H_2$  value is characteristic of a strong interaction process, counter compensated by the large negative  $\Delta S_2$  value. In the purified NorM\_PS preparation, phospholipid molecules were detected (data not shown), which could be negatively charged. Thus, the weak binding of DAPI to NorM\_PS could be due to the interaction between DAPI and the bound lipids.

**Quantitative Ligand Binding**—So far, only limited information regarding substrate binding is available for the MATE transporters. The binding between DinF-BH and rhodamine 6G was studied using fluorescence polarization, and the  $K_d$  value was determined to be 3.1  $\mu\text{M}$  (10). Using the same technique, another quantitative binding study was performed on NorM\_VC, and the  $K_d$  value for rhodamine 6G and doxorubicin binding to NorM\_VC was 2.1 and 1.0  $\mu\text{M}$ , respectively (8). For many other multidrug transporters, dissociation constants in the micromolar range were reported for substrate binding (28–32). One of the reports regarding MdfA is of particular interest, because MdfA is a multidrug transporter of *E. coli*, belonging to the major facilitator superfamily, which shares some structural and functional similarities with NorM\_PS. MdfA also has 12 TMHs and functions in the monomeric form. The  $K_d$  value of MdfA and chloramphenicol was determined to be 75  $\mu\text{M}$  using ITC (32). The binding affinity is lower than the observed affinity between NorM\_PS and DAPI in our study. This difference could be due to the dominating binding interaction. In the case of MdfA, the carboxyl side chain of Asp-34 forms two H-bonds with the O4 and O5 hydroxyl groups of chloramphenicol (32), whereas in this study, the high-affinity binding between NorM\_PS and DAPI is supposed to be caused by electrostatic interactions.

In this study, two independent methods, spectrofluorometric titration and ITC, were applied to quantify substrate binding. Only one binding event was identified using spectrofluorometric titration and the corresponding affinity is about 5 times



lower than the  $K_d$  obtained from ITC. This difference is easy to understand because the binding event observed in the spectrofluorometric titration had a contribution from the low-affinity binding site, but due to the limitations of our experimental conditions, it is difficult to resolve the two binding events using this method.

### Structural Aspects

**Asp-38 Is Involved in  $H^+$  Translocation**—Asp-41<sup>PfMATE</sup> (corresponding to Asp-38<sup>NorM\_PS</sup>) was reported to be involved in  $H^+$  translocation by changing its protonation state: the change may trigger the reorganization of the interaction network, thereby inducing the structural transition between the straight and bent conformations of TMH1 (11). Moreover, another orthologue of Asp-38<sup>NorM\_PS</sup>, Asp-40<sup>DinF-BH</sup> was proposed to be a competition site for substrate and  $H^+$  (10). From our study, Asp-38 of NorM\_PS seems to possess a crucial function but we have not obtained any evidence to support a role in substrate binding. The substitution of Asp by Asn led to a deficiency of DAPI extrusion, but the DAPI binding was hardly affected (Figs. 5*a* and 7*a*). This result suggests that Asp-38 is not required for DAPI binding. Therefore it is unlikely that there is a direct competition between the substrate and proton for Asp-38. However, D38N did not show any  $H^+$  translocation in the antiport assay (Fig. 3), which can be the reason for the loss of its function.

**Critical Role of Glu-257**—Among the NorM subfamily proteins, the glutamate residue in TMH7 is highly conserved, and Glu-251<sup>NorM\_VP</sup>, Glu-255<sup>NorM\_VC</sup>, and Glu-261<sup>NorM\_NG</sup> have been proposed to be important. Electron density for a  $Cs^+$  ion was observed in the x-ray structure of NorM\_VC between Glu-255 and Asp-371; in NorM\_NG, Glu-261 and Tyr-294 could coordinate a  $Na^+$  ion (8, 9, 33). Unlike both proteins mentioned above, NorM\_PS is  $H^+$  dependent, and Glu-257 in NorM\_PS is likely to stabilize the protein structurally as well as involved in DAPI binding.

Of the three different variants constructed (E257A, E257Q, and E257D), only E257D could be purified successfully using our standard procedure. This result indicates that the negative charge is important for structural stability. Given that Glu-257 is located in the middle of TMH7, it is possible that Glu-257 stabilizes the protein by interacting with the N-bundle or the amino acid residues close by via electrostatic interactions.

No high-affinity binding to DAPI could be observed for E257D, indicating a participation in substrate binding. But the question whether Glu-257 plays a role in  $H^+$  translocation remains unanswered.

**Proposed High-affinity DAPI Binding Site**—In contrast to the WT protein, a resulting endothermic process in the binding of DAPI to D373N as well as to E257D was observed by ITC. This observation might be caused by a protein conformational change required for the formation of the 1:1 DAPI-protein complex. It is thus not surprising that the affinity became lower than in the WT protein. This assumption is supported by the results of the spectrofluorometric titrations. The blue shift in the emission spectra of DAPI was smaller when bound to D373N and E257D compared to the WT protein (Fig. 5*c*), suggesting a less hydrophobic environment for DAPI.

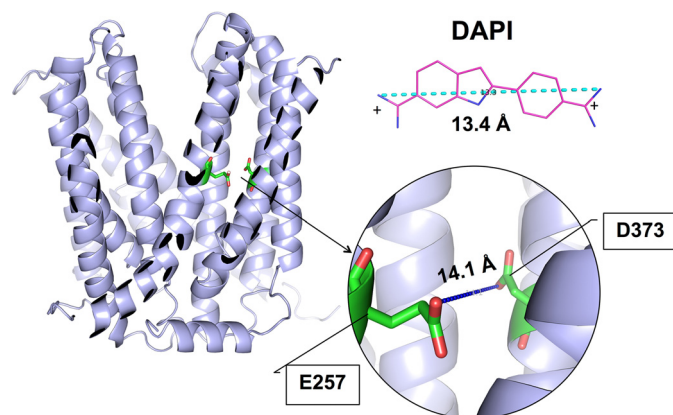


FIGURE 8. **Identification of the high-affinity DAPI binding site.** The homology model of NorM\_PS is shown in light blue, Asp-373 and Glu-257 are shown in green, the oxygen atoms are in red. DAPI is shown as stick model, carbon and nitrogen atoms in magenta and blue, respectively.

The C-bundle cavity lined by Asp-373, Glu-257, and many hydrophobic amino acid residues is proposed to be the high-affinity DAPI binding site for three reasons. (i) The distance between Asp-373 and Glu-257 is  $\sim 14$  Å, and the distance between the two positive charges of DAPI molecule was 13.4 Å (Fig. 8). Although the distance was calculated based on an outward-facing homology model, and for mechanistic reasons, high-affinity binding was to be expected to take place in a different conformation such as in the postulated inward-facing state, no dramatic change of the distance in the inward-facing conformation should be expected. Moreover, the fact that the variant E257D presented a different binding behavior shows the importance of the distance. (ii) The results of fluorescence titration also provide evidence for this assumption. Glu-257 and Asp-373 are surrounded by many hydrophobic amino acid residues (Val-254, Phe-255, Ala-256, Ile-260, Phe-261, Phe-290, Met-291, Val-374, Val-375, Val-377, Leu-294, Leu-434, and Phe-398), which confirms the conclusion that DAPI is exposed to a very hydrophobic environment when bound to the protein. (iii) The observation of an exothermic binding in ITC is likely to imply charge neutralization. If Glu-257 and Asp-373 are part of the binding pocket, electrostatic interactions would dominate the binding process, and the charge neutralization should be the consequence. Taken together, Glu-257 and Asp-373 should be major contributors to the high-affinity DAPI binding site.

Summarizing, we can say that DAPI binds to solubilized NorM\_PS with two affinities, and residues Glu-257 and Asp-373 are directly involved in the high-affinity binding event. For the low-affinity binding event, so far no evidence has been obtained in favor of a physiological function. Kinetic binding studies will undoubtedly increase our understanding of these two binding events.

### Experimental Procedures

**Bacterial Strains and Expression Vectors**—The *E. coli* strain DH5 $\alpha$  (Invitrogen) was used for cloning and site-directed mutagenesis, and the *E. coli* strain TOP10 (Invitrogen) was used for heterologous protein production. For functional studies, *E. coli* strain KAM32 (a kind gift of Dr. Teruo Kuroda from Okayama University) was used, which lacks AcrB and YdhE

transporters and thus becomes drug-hypersensitive (34). For heterologous protein production in *E. coli*, a modified pBAD vector (Invitrogen), pBADA2, which contains a tobacco etch virus protease cleavage site and a decahistidine tag (His tag) attached at the C terminus of the target protein, was used (35).

**Cloning of Genes**—Phusion DNA polymerase (Finnzymes) was used for regular PCR. The primer sequences are listed in supplemental Table S1. The gene encoding the NorM\_PS (GenBank™ EHY79494.1) was amplified from the genomic DNA of *P. stutzeri* strain ZoBell (ATCC14405). The resulting 1623-bp PCR product was cloned into the pJET1.2 vector using CloneJET PCR cloning kit (Thermo Fisher Scientific). Subsequently, a second PCR was performed to add BamHI and EcoRI restriction enzyme sites to flank the target gene. The resulting PCR product was digested with BamHI-EcoRI endonucleases (Thermo Fisher Scientific) and ligated into the BamHI and EcoRI sites of pBADA2. Site-directed mutations were constructed using the QuikChange Lightning site-directed mutagenesis kit (Agilent Technologies). All constructs were checked by DNA sequencing (SeqLab).

**Protein Expression and Purification**—The expression vector pBADA2-NorM\_PS was transformed into TOP10 cells for large-scale production or into KAM32 cells for MIC tests. After selection on agar plates, a single colony was used to inoculate 50 ml of LB medium containing 50 µg/ml of carbenicillin and incubated at 37 °C overnight. 25 ml of this pre-culture was used to inoculate 2 liters of LB medium. The culture was incubated at 37 °C at 180 rpm until the optical density (OD) at 600 nm reached 0.5–0.7. The protein production was induced by addition of 0.05% (w/v) L-arabinose at 37 °C for 2.5 h. To detect the expression, a 1-ml sample was harvested by centrifugation and the pellet was resuspended in 100 µl of 10% SDS. After 30 min of incubation at room temperature, the sample was centrifuged (14,000 × g, room temperature, 30 min). 15 µl of the supernatant were subsequently mixed with 5 µl of NuPAGE® SDS Sample Buffer (×4) (Invitrogen), and subsequently analyzed on Novex 4–12% Bistris gels (Invitrogen) by SDS-PAGE and evaluated by Western blot using an alkaline phosphatase-conjugated anti-His antibody (Sigma) according to the manufacturer's instructions.

Cells were harvested by centrifugation (10,500 × g, 4 °C, 20 min) and resuspended in the lysis buffer (20 mM HEPES-NaOH, 100 mM NaCl, pH 7.4, 2 mM phenylmethylsulfonyl fluoride (PMSF; Carl Roth)), at a ratio of 1 g of wet cell/5 ml of buffer, and a small amount of DNase I (Roche Applied Science) was added. The cells were disrupted twice by passing through an M-110LA microfluidizer (Microfluidics) under ice at 8,000 psi. The cell debris was removed by centrifugation (14,000 × g, 4 °C, 1 h). The resulting membrane vesicles were collected from the lysate supernatant after ultracentrifugation (145,000 × g, 4 °C, 2 h). The pelleted vesicles were resuspended in 20 mM HEPES-NaOH, 100 mM NaCl, pH 7.4. The total protein content in the membrane fraction was determined using the BCA assay (Pierce) according to the manufacturer's instructions. The final protein concentration of the vesicle suspension was adjusted to 10 mg/ml. The vesicles were frozen in liquid nitrogen and stored at –80 °C.

All solubilization and purification steps were performed at 4 °C. Membranes were solubilized in the presence of 2% (w/v) β-DDM (Glycon Chemicals) for 1 h with slow agitation. The insoluble membrane fraction was removed by ultracentrifugation (170,000 × g, 4 °C, 1 h). The supernatant containing the solubilized NorM\_PS was mixed with nickel-nitrilotriacetic acid-agarose beads (Qiagen) at a ratio of 200 mg of total membrane protein/ml of beads. The nickel-nitrilotriacetic acid beads were pre-equilibrated with binding buffer (20 mM HEPES-NaOH, 300 mM NaCl, 0.025% (w/v) β-DDM, and 30 mM imidazole, pH 7.4). The mixture was incubated with slow agitation for 1 h. After incubation, beads with bound proteins were collected in a gravity column and washed with 20 column volumes (CV) of binding buffer. Subsequently, the beads were further washed with 10 CV of washing buffer I (binding buffer + 50 mM imidazole), 5 CV of washing buffer II (binding buffer + 80 mM imidazole), and the target protein was eluted with 8 CV of elution buffer (20 mM HEPES-NaOH, 100 mM of sodium lactate, 300 mM imidazole-HCl, and 0.025% (w/v) β-DDM, pH 7.4). The eluted fraction was concentrated 30-fold in an Amicon concentrator with 50-kDa cut-off membrane (Millipore) and loaded onto a Superdex 200 10/300 column (GE Healthcare) pre-equilibrated with the NorM\_PS sample buffer (20 mM HEPES-NaOH, 11 mM sodium lactate, and 0.025% (w/v) β-DDM, pH 7.4). For analytical chromatography, a Superdex 200 PC 3.2/30 column (GE Healthcare) was used to investigate the homogeneity of the purified protein.

**Size Exclusion Chromatography Coupled to Multi-angle Light Scattering**—The oligomeric state of NorM\_PS was determined by SEC-MALS and differential refractive-index measurements (Viscotek SEC-MALS 20, Malvern). Prior to the NorM\_PS run, the system was calibrated with 3.5 mg/ml of BSA sample in the NorM\_PS sample buffer. 100 µl of the purified protein (3.8 mg/ml) were loaded onto a Superdex 200 10/300 column. For data evaluation, the molar extinction coefficient of NorM\_PS at 280 nm ( $\epsilon_{280}$ ) ( $63,745 \text{ M}^{-1} \text{ cm}^{-1}$ ) was used. The specific refractive index increment of the protein was  $0.187 \text{ ml g}^{-1}$ , the  $\epsilon_{280}$  and refractive index increment of β-DDM were  $0.001 \text{ ml mg}^{-1} \text{ cm}^{-1}$  and  $0.133 \text{ ml g}^{-1}$ , respectively, all values were taken from the literature (20). The calculation was performed using the “Copolymer method” using the software provided by the manufacturer (Malvern OmniSEC).

**Determination of Protein Concentration**—The protein concentration was roughly measured by the BCA protein assay according to the manufacturer's instructions. To precisely determine the protein concentration, quantitative amino acid analysis (Functional Genomics Center Zurich) was performed. 1 mg of protein determined by the BCA test corresponded to 1.24 mg. The resulting factor of 1.24 was used to correct all future values obtained from the BCA assay for further ITC, DSC, and fluorescence studies; the molecular mass of NorM\_PS was 53,066.7 Da based on its amino acid composition.

**Drug Resistance Assay**—The drug susceptibility test was performed based on established protocols with minor modifications (36). Freshly transformed negative control cells (KAM32 cells + empty pBADA2 vector) and test cells (KAM32 cells + pBADA2-NorM\_PS vector) were grown in LB at 37 °C until the  $A_{600}$  reached 0.5 and induced with 0.05% (w/v) L-arabinose.



After incubation for 45 min, the cells were used to inoculate 1 ml of test medium (LB medium containing 0.005% (w/v) L-arabinose, 50  $\mu\text{g}/\text{ml}$  of carbenicillin, and different concentrations of antibiotics, drugs, and other toxic compounds). The inoculum corresponded to  $10^5$ – $10^6$  colony-forming units/ml of media. Cells were incubated at 37 °C for 24 h, and the growth was monitored by measuring  $A_{600}$ .

The drug resistance test was also performed using LB without NaCl (FORMEDIUM) to study the cation dependence of the transport. We defined the MIC as the lowest concentrations of toxic compounds that inhibit the visible growth of cells after overnight incubation under our experimental conditions. DAPI, doxorubicin, daunorubicin, tetracycline, kanamycin, gentamycin, benzamidine, streptomycin, chloramphenicol, ciprofloxacin, norfloxacin, rhodamine 6G, acriflavine, propidium iodide, berberine, ethidium bromide, and tetraphenylphosphonium chloride were tested. All assays were repeated at least three times independently.

**DAPI/ $H^+$  Antiport Assay**—Everted membrane vesicles were prepared for the antiport assay. pBADA2 and pBADA2-NorM\_PS were transformed into *E. coli* KAM32 strain. After 2.5 h of induction, cells were harvested and the everted vesicles were prepared according to Ref. 37. Total protein concentration was measured by the BCA assay and adjusted to 20 mg/ml. Aliquots of 200  $\mu\text{l}$  were frozen in liquid nitrogen and stored at  $-80$  °C.

The antiport assay was conducted at 25 °C in a reaction mixture (1 ml) consisting of modified TCS buffer (5 mM Tris-HCl, 140 mM choline chloride, 5 mM  $\text{MgCl}_2$ , pH 7.4) containing 2  $\mu\text{M}$  acridine orange (Sigma) and 400  $\mu\text{g}$  of total protein in everted vesicles. 10  $\mu\text{l}$  of 1 M Na-DL-lactate (Fluka) was added to the mixture to initiate respiration. 2.5  $\mu\text{l}$  of 20 mM DAPI dihydrochloride (Sigma) were added after fluorescence quenching reached a steady state. The sample was continuously stirred during the measurement. All fluorescence measurements were performed with a Hitachi F-4500 fluorescence spectrophotometer in the time-scan configuration, with excitation at 495 nm and emission at 530 nm. Slit width was 5 nm for both excitation and emission, PMT voltage was set to 700 V. DAPI concentration was determined by measuring its absorption, with  $\epsilon_{340} = 30,000 \text{ M}^{-1} \text{ cm}^{-1}$  (in water) (38).

**Differential Scanning Calorimetry**—The DSC measurements were performed using a VP-Capillary DSC system (MicroCal, Malvern, Inc.). Typically, 350  $\mu\text{l}$  of protein in the NorM\_PS sample buffer at a concentration of 25  $\mu\text{M}$  was injected into the cell (MicroCal, Malvern, Inc.). Scanning was performed from 10 to 85 °C at a rate of 120 °C/h in the low feedback mode with a 5-min pre-equilibration phase. The system pressure was provided by  $\text{N}_2$  and about 60 psi during measurement. Data analysis was processed using Origin 7.0 software (Microcal Origin); thermograms were corrected by subtracting buffer-only blank scans.

**Spectrofluorometry**—The fluorescent binding assay was carried out by spectrofluorometric titrations at 25 °C. 0.5  $\mu\text{M}$  DAPI in the NorM\_PS sample buffer was titrated with concentrated protein samples (up to 250  $\mu\text{M}$ ). Fluorescence measurements were done with a Hitachi F-4500 fluorescence spectrophotometer in the wavelength scan configuration. Excitation wave-

length was 360 nm, and emission wavelength was measured from 380 to 580 nm. Emission at 450 nm was used to record the excitation spectra and for titration analysis. To minimize inner filter effects, a 5  $\times$  5-mm quartz cuvette (101-058-40, Hellma Analytics) was used. Corresponding absorption spectra before and after titrations were conducted in absorption cuvettes (104-5-K-40, Hellma Analytics) with 5-nm light path. Under the chosen condition, the concentration of bound DAPI was always small and thus neglectable compared with that of the total concentration. Volume change corrected intensities at 450 nm together with associated total DAPI concentration were evaluated according to the Henderson-Hasselbach equation based on a 1:1 binding equilibrium. The dissociation constants,  $K_d$ , were given as mean values of three independent titrations.

**Isothermal Titration Calorimetry**—ITC measurements were performed at 25 °C with a VP-ITC calorimeter consisting of a 1.45-ml reaction cell and a 278- $\mu\text{l}$  syringe (Malvern, MicroCal, Inc.). The experimental conditions for each measurement are specified in figure legends. To achieve a higher concentration range, two successive titrations with the same ligand solution were performed and combined by the program CONCAT (Malvern, MicroCal, Inc.). The general settings of the instrument were as follows: data interval was 360 s, the stirring speed was 351 rpm, and gain mode was “high.”

Data evaluation was employed using software (MicroCal Origin) based on the “two binding sites” model. All the variants titrations were evaluated in the same way as the WT protein titration. The 1st injection usually had an inaccuracy in volume, so it was not taken into consideration for further analysis and marked with “m” in Figs. 6 and 7.

**Homology Modeling**—The homology model of NorM\_PS was constructed using the web-based protein structure modeling server I-TASSER (39–41). The three-dimensional model was generated on the basis of the x-ray structure of the NorM\_VC protein (Protein Data Bank code 3MKU), which shares a 43% overall sequence identity with NorM\_PS.

**Author Contributions**—H. M. supervised research; L. N., E. G., J. W., and H. M. designed research; L. N., V. M., and H. X. performed the research; L. N. and E. G. analyzed data; L. N. and E. G. wrote the manuscript.

**Acknowledgments**—We thank Cornelia Muenke for excellent technical assistance, Lisa Joedicke for the assistance with SEC-MALS, Helga Husmann for helping in producing figures, and Dr. Marco Marenchino (Malvern) for providing CONCAT.

## References

- Wong, K., Ma, J., Rothnie, A., Biggin, P. C., and Kerr, I. D. (2014) Towards understanding promiscuity in multidrug efflux pumps. *Trends Biochem. Sci.* **39**, 8–16
- Noble, R. C., and Overman, S. B. (1994) *Pseudomonas stutzeri* infection: a review of hospital isolates and a review of the literature. *Diagn. Microbiol. Infect. Dis.* **19**, 51–56
- Putman, M., van Veen, H. W., and Konings, W. N. (2000) Molecular properties of bacterial multidrug transporters. *Microbiol. Mol. Biol. Rev.* **64**, 672–693
- Hvorup, R. N., Winnen, B., Chang, A. B., Jiang, Y., Zhou, X.-F., and Saier,



- M. H., Jr. (2003) The multidrug/oligosaccharidyl-lipid/polysaccharide (MOP) exporter superfamily. *Eur. J. Biochem.* **270**, 799–813
5. Brown, M. H., Paulsen, I. T., and Skurray, R. A. (1999) The multidrug efflux protein NorM is a prototype of a new family of transporters. *Mol. Microbiol.* **31**, 394–395
6. Omote, H., Hiasa, M., Matsumoto, T., Otsuka, M., and Moriyama, Y. (2006) The MATE proteins as fundamental transporters of metabolic and xenobiotic organic cations. *Trends Pharmacol. Sci.* **27**, 587–593
7. Kuroda, T., and Tsuchiya, T. (2009) Multidrug efflux transporters in the MATE family. *Biochim. Biophys. Acta* **1794**, 763–768
8. He, X., Szewczyk, P., Karyakin, A., Evin, M., Hong, W.-X., Zhang, Q., and Chang, G. (2010) Structure of a cation-bound multidrug and toxic compound extrusion transporter. *Nature* **467**, 991–994
9. Lu, M., Symersky, J., Radchenko, M., Koide, A., Guo, Y., Nie, R., and Koide, S. (2013) Structures of a Na<sup>+</sup>-coupled, substrate-bound MATE multidrug transporter. *Proc. Natl. Acad. Sci. U.S.A.* **110**, 2099–2104
10. Lu, M., Radchenko, M., Symersky, J., Nie, R., and Guo, Y. (2013) Structural insights into H<sup>+</sup>-coupled multidrug extrusion by a MATE transporter. *Nat. Struct. Mol. Biol.* **20**, 1310–1317
11. Tanaka, Y., Hipolito, C. J., Maturana, A. D., Ito, K., Kuroda, T., Higuchi, T., Katoh, T., Kato, H. E., Hattori, M., Kumazaki, K., Tsukazaki, T., Ishitani, R., Suga, H., and Nureki, O. (2013) Structural basis for the drug extrusion mechanism by a MATE multidrug transporter. *Nature* **496**, 247–251
12. Du, D., van Veen, H. W., and Luisi, B. F. (2015) Assembly and operation of bacterial tripartite multidrug efflux pumps. *Trends Microbiol.* **23**, 311–319
13. Lalucat, J., Bennisar, A., Bosch, R., García-Valdés, E., and Palleroni, N. J. (2006) Biology of *Pseudomonas stutzeri*. *Microbiol. Mol. Biol. Rev.* **70**, 510–547
14. Wei, Y., Li, H., and Fu, D. (2004) Oligomeric state of the *Escherichia coli* metal transporter YiiP. *J. Biol. Chem.* **279**, 39251–39259
15. Yernool, D., Boudker, O., Foltá-Stogniew, E., and Gouaux, E. (2003) Trimeric subunit stoichiometry of the glutamate transporters from *Bacillus caldolenax* and *Bacillus stearothermophilus*. *Biochemistry* **42**, 12981–12988
16. Hayashi, Y., Matsui, H., and Takagi, T. (1989) Membrane protein molecular weight determined by low-angle laser light-scattering photometry coupled with high-performance gel chromatography. *Methods Enzymol.* **172**, 514–528
17. Jasti, J., Furukawa, H., Gonzales, E. B., and Gouaux, E. (2007) Structure of acid-sensing ion channel 1 at 1.9 Å resolution and low pH. *Nature* **449**, 316–323
18. Vásquez, V., Cortes, D. M., Furukawa, H., and Perozo, E. (2007) An optimized purification and reconstitution method for the MscS channel: strategies for spectroscopical analysis. *Biochemistry* **46**, 6766–6773
19. White, J. F., Grodnitzky, J., Louis, J. M., Trinh, L. B., Shiloach, J., Gutierrez, J., Northup, J. K., and Grisham, R. (2007) Dimerization of the class A G protein-coupled neurotensin receptor NTS1 alters G protein interaction. *Proc. Natl. Acad. Sci. U.S.A.* **104**, 12199–12204
20. Slotboom, D. J., Duurkens, R. H., Olieman, K., and Erkens, G. B. (2008) Static light scattering to characterize membrane proteins in detergent solution. *Methods* **46**, 73–82
21. Cools, A. A., and Janssen, L. H. (1986) Fluorescence response of acridine orange to changes in pH gradients across liposome membranes. *Experientia* **42**, 954–956
22. Härd, T., Fan, P., and Kearns, D. R. (1990) A Fluorescence study of the binding of Hoechst 33258 and DAPI to halogenated DNAs. *Photochem. Photobiol.* **51**, 77–86
23. Mazzini, A., Cavatorta, P., Iori, M., Favilla, R., and Sartor, G. (1992) The binding of 4',6-diamidino-2-phenylindole to bovine serum albumin. *Biophys. Chem.* **42**, 101–109
24. Favilla, R., Stecconi, G., Cavatorta, P., Sartor, G., and Mazzini, A. (1993) The interaction of DAPI with phospholipid vesicles and micelles. *Biophys. Chem.* **46**, 217–226
25. Nishino, K., and Yamaguchi, A. (2001) Analysis of a complete library of putative drug transporter genes in *Escherichia coli*. *J. Bacteriol.* **183**, 5803–5812
26. Islam, S. T., and Lam, J. S. (2013) Wzx flippase-mediated membrane translocation of sugar polymer precursors in bacteria. *Environ. Microbiol.* **15**, 1001–1015
27. Jin, Y., Nair, A., and van Veen, H. W. (2014) Multidrug transport protein NorM from *Vibrio cholerae* simultaneously couples to sodium- and proton-motive force. *J. Biol. Chem.* **289**, 14624–14632
28. Sikora, C. W., and Turner, R. J. (2005) Investigation of ligand binding to the multidrug resistance protein EmrE by isothermal titration calorimetry. *Biophys. J.* **88**, 475–482
29. Vázquez-Laslop, N., Markham, P. N., and Neyfakh, A. A. (1999) Mechanism of ligand recognition by BmrR, the multidrug-responding transcriptional regulator: mutational analysis of the ligand-binding site. *Biochemistry* **38**, 16925–16931
30. Markham, P. N., Ahmed, M., and Neyfakh, A. A. (1996) The drug-binding activity of the multidrug-responding transcriptional regulator BmrR resides in its C-terminal domain. *J. Bacteriol.* **178**, 1473–1475
31. Lewinson, O., and Bibi, E. (2001) Evidence for simultaneous binding of dissimilar substrates by the *Escherichia coli* multidrug transporter MdfA. *Biochemistry* **40**, 12612–12618
32. Heng, J., Zhao, Y., Liu, M., Liu, Y., Fan, J., Wang, X., Zhao, Y., and Zhang, X. C. (2015) Substrate-bound structure of the *E. coli* multidrug resistance transporter MdfA. *Cell Res.* **25**, 1060–1073
33. Otsuka, M., Yasuda, M., Morita, Y., Otsuka, C., Tsuchiya, T., Omote, H., and Moriyama, Y. (2005) Identification of essential amino acid residues of the NorM Na<sup>+</sup>/multidrug antiporter in *Vibrio parahaemolyticus*. *J. Bacteriol.* **187**, 1552–1558
34. Chen, J., Morita, Y., Huda, M. N., Kuroda, T., Mizushima, T., and Tsuchiya, T. (2002) VmrA, a member of a novel class of Na<sup>+</sup>-coupled multidrug efflux pumps from *Vibrio parahaemolyticus*. *J. Bacteriol.* **184**, 572–576
35. Kaur, J., Olkhova, E., Malviya, V. N., Grell, E., and Michel, H. (2014) A L-lysine transporter of high stereoselectivity of the amino acid-Polyamine-organocation (APC) superfamily: production, functional characterization, and structure modeling. *J. Biol. Chem.* **289**, 1377–1387
36. Wiegand, I., Hilpert, K., and Hancock, R. E. (2008) Agar and broth dilution methods to determine the minimal inhibitory concentration (MIC) of antimicrobial substances. *Nat. Protoc.* **3**, 163–175
37. Rycovska, A., Hatahet, L., Fendler, K., and Michel, H. (2012) The nitrite transport protein NirC from *Salmonella typhimurium* is a nitrite/proton antiporter. *Biochim. Biophys. Acta* **1818**, 1342–1350
38. Green, F. J. (1990) *The Sigma-Aldrich Handbook of Stains, Dyes, and Indicators*, Aldrich Chemical Co., Milwaukee, WI
39. Roy, A., Kucukural, A., and Zhang, Y. (2010) I-TASSER: a unified platform for automated protein structure and function prediction. *Nat. Protoc.* **5**, 725–738
40. Zhang, Y. (2008) I-TASSER server for protein 3D structure prediction. *BMC Bioinformatics* **9**, 40
41. Yang, J., Zhang, W., He, B., Walker, S. E., Zhang, H., Govindarajoo, B., Virtanen, J., Xue, Z., Shen, H.-B., and Zhang, Y. (2015) Template-based protein structure prediction in CASP11 and retrospect of I-TASSER in the last decade. *Proteins* **10.1002/prot.24918**

**Identification of the High-affinity Substrate-binding Site of the Multidrug and Toxic Compound Extrusion (MATE) Family Transporter from *Pseudomonas stutzeri***

Laiyin Nie, Ernst Grell, Viveka Nand Malviya, Hao Xie, Jingkang Wang and Hartmut Michel

*J. Biol. Chem.* 2016, 291:15503-15514.

doi: 10.1074/jbc.M116.728618 originally published online May 27, 2016

---

Access the most updated version of this article at doi: [10.1074/jbc.M116.728618](https://doi.org/10.1074/jbc.M116.728618)

Alerts:

- [When this article is cited](#)
- [When a correction for this article is posted](#)

[Click here](#) to choose from all of JBC's e-mail alerts

Supplemental material:

<http://www.jbc.org/content/suppl/2016/05/27/M116.728618.DC1>

This article cites 40 references, 11 of which can be accessed free at <http://www.jbc.org/content/291/30/15503.full.html#ref-list-1>